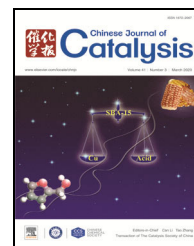


available at www.sciencedirect.comjournal homepage: www.elsevier.com/locate/chnjc

Article

Selective oxidation of glycerol with oxygen in base-free solution over N-doped-carbon-supported Sb@PtSb₂ hybrid

Lihua Yang^a, Tianqu He^a, Chujun Lai^a, Ping Chen^a, Zhaoyin Hou^{a,b,*}^a Key Laboratory of Biomass Chemical Engineering of Ministry of Education, Department of Chemistry, Zhejiang University, Hangzhou 310028, Zhejiang, China^b Center of Chemistry for Frontier Technologies, Department of Chemistry, Zhejiang University, Hangzhou 310028, Zhejiang, China

ARTICLE INFO

Article history:

Received 4 July 2019

Accepted 6 August 2019

Published 5 March 2020

Keywords:

Glycerol

Oxidation

Base-free solution

Sb@PtSb₂

Alloy

ABSTRACT

Selective oxidation of glycerol with molecular oxygen in base-free aqueous solutions has become a hot topic, as the rapidly increasing production of biodiesel is creating a surplus of glycerol. In this work, an N-doped-carbon-supported core-shell structured Sb@PtSb₂ hybrid catalyst was prepared via a facile synthesis route, in which a mixture of glucose, melamine, and SbCl₃ (Sb-NC) was pyrolyzed, then impregnated with Pt by immersion in an aqueous solution of H₂PtCl₆, and further treated in hydrogen flow. Characterization of the catalyst products indicated that introducing SbCl₃ can increase the surface area of the binary glucose + melamine pyrolyzed support (NC), and Sb@PtSb₂ hybrids could be formed on the surface of an Sb-NC support during hydrogen treatment at 700 °C. It was found that the Sb@PtSb₂/NC catalyst was more active for the selective oxidation of glycerol in a base-free aqueous solution than Sb-free NC-supported Pt (Pt/NC). Further characterization also indicated that the promising performance of Sb@PtSb₂/NC might be attributed to its enhanced oxygen activation.

© 2020, Dalian Institute of Chemical Physics, Chinese Academy of Sciences.

Published by Elsevier B.V. All rights reserved.

1. Introduction

Biodiesel is a renewable, biodegradable fuel manufactured domestically from vegetable oils, animal fats, or recycled restaurant grease. It can be used in pure form or it may be blended with petroleum diesel at any concentration in most injection pump diesel engines. Glycerol is formed as a byproduct during the production of biodiesel, and the amount of glycerol produced has increased quickly with the rapid expansion of biodiesel applications [1,2]. It was estimated that the production of glycerol in 2020 will be six times higher than demand [2].

In the past decade, much effort has been devoted to developing processes to convert glycerol into valuable products

[3–7]. Among these processes, selective oxidation of glycerol with molecular oxygen over heterogeneous catalysts to form dihydroxyacetone (DHA), glyceric acid (GLYA), glyceraldehyde (GLYHD), hydroxypyruvic acid (HPYA), and lactic acid has become a hot topic both in academic research and industrial applications [8–13]. Based on previously published works, it was generally concluded that the oxidation of glycerol with molecular oxygen is a structure-sensitive process, in which the reaction mechanism and product distribution vary significantly with different conditions (pH, temperature, and substrate to metal ratio) [11–22].

The use of carbon-supported Pt catalysts has been widely reported in the base-free aqueous liquid-phase oxidation of

* Corresponding author. E-mail: zyhou@zju.edu.cn

This work was financially supported by the National Natural Science Foundation of China (21773206 and 21473155) and Natural Science Foundation of Zhejiang Province (L12B03001).

DOI: S1872-2067(19)63476-5 | <http://www.sciencedirect.com/science/journal/18722067> | Chin. J. Catal., Vol. 41, No. 3, March 2020

glycerol [23,24]. But the deactivation of nano-sized Pt catalysts has often been reported during the selective oxidation of alcohols due to the weaker interactions between Pt and the carbon support, over-oxidation of surface Pt nanoparticles (NPs), and/or the strong adsorption of organic carboxylic acids [23–25].

Recently, it was recommended that adding and/or alloying Pt with another metal is an effective approach to preventing the deactivation of Pt NPs. For example, Au- [15,26–28], Bi- [8,9,29], Ru- [30], Sn- [31,32], Ni- [33], Co- [34] and Sb- [35,36] promoted or alloyed Pt catalysts have been used for selective oxidation in the liquid phase. At the same time, it was also reported that N atoms in the framework of the carbon support can donate electrons to Pt, thereby enhancing the interactions between the support and the metal, and thus improving the dispersion, activity, and stability of Pt, and/or generating new active sites [24,37–39].

Previous work in our laboratory showed that a PtSb alloy supported on multi-walled carbon nanotubes (MWCNTs) was highly active for the selective oxidation of glycerol in base-free aqueous solutions and that a PtSb alloy can hinder the cleavage of C–C bonds [35]. Recent works published by other groups have also confirmed that a Pt–Sb alloy was both more active and selective for the formation of DHA [36,40]. But the fabrication of PtSb alloy NPs on MWCNTs is a tedious, time-consuming, and dangerous process [41], and commercial MWCNT supports are expensive.

In this work, we report a facile preparation method for the direct fabrication of Sb@PtSb₂ hybrids with a core-shell structure on N-doped carbon via simple pyrolysis of a mixture of glucose, melamine, and SbCl₃, according to the reaction scheme shown in Fig. 1. Furthermore, this Sb@PtSb₂/NC catalyst was characterized and tested for the selective oxidation of glycerol in base-free aqueous solutions.

2. Experimental

2.1. Catalyst preparation

2.1.1. Sb@PtSb₂/NC

Specific amounts of glucose, melamine, and SbCl₃ (with a mass ratio of 6:6:1) were added and mixed manually in a ceramic mortar for 1 h, and then the mixture was dried in vacuum at 80 °C overnight. After that, the mixture was transferred to a quartz furnace and heated at 700 °C for 4 h (with a heating

rate of 5 °C/min) under a nitrogen flow of 20 mL/min. The obtained black powder was treated in 50 mL HCl (37 wt.%) under stirring for 6.0 h to remove the soluble species. The acid-treated solid sample was then filtered out, washed thoroughly with distilled water, and dried in vacuum at 60 °C overnight. The prepared sample is denoted as Sb/NC. Secondly, Sb/NC (1 g) was dispersed in a 7-mL aqueous solution of H₂PtCl₆ (0.01 g Pt/mL) under stirring, and further treated in an ultrasonic bath for 30 minutes. This suspension was then dried at 60 °C, and the dried black powder was treated at 700 °C under hydrogen flow for 1 h. The final catalyst is denoted as Sb@PtSb₂/NC. The N-free Sb@Pt/C catalyst was prepared by following the same procedures as above without the addition of melamine in the feed.

2.1.2. Pt/NC

Specific amounts of glucose and melamine (with a mass ratio of 1:1.5, in order to ensure the same N content in both Pt/NC and Sb@PtSb₂/NC) were added and mixed manually in a ceramic mortar for 1 h, and then the mixture was dried in vacuum at 80 °C overnight. After that, the mixture was transferred to a quartz furnace and heated at 700 °C for 4 h (with a heating rate of 5 °C/min) under a nitrogen flow of 20 mL/min. The prepared sample is denoted as NC. Secondly, NC (1 g) was dispersed in a 7-mL aqueous solution of H₂PtCl₆ (0.01 g Pt/mL) under stirring. The suspension was then treated in an ultrasonic wave bath for 30 minutes. After that, the suspension was dried at 60 °C, and the dried black powder was further treated at 700 °C under hydrogen flow for 1 h. The final catalyst is denoted as Pt/NC. N-free Pt/C catalyst was prepared by following the same procedures used to produce Pt/NC without the addition of melamine in the feed.

2.2. Catalyst characterization

The real content of Sb and Pt in the prepared catalysts were measured using the following procedures. A sample (0.5 g) was treated in air from 25 to 900 °C (with a heating rate of 5 °C/min), and then the residual solids were dissolved with 50 mL of aqua regia. Metal ions in the resulting solution were detected via inductively coupled plasma-atomic emission spectroscopy (ICP, Plasma-Spec-II spectrometer), and these data are summarized in Table 1.

The texture and structure of all samples were characterized by N₂ adsorption measurements at –196 °C in a static volumetric apparatus (Micromeritics ASAP2020). Samples were first treated at 250 °C for 4 h under high vacuum. The specific surface area was calculated using the Brunner-Emmet-Teller (BET) method and pore size distributions were calculated using the Barrett-Joyner-Halenda (BJH) method. X-ray diffraction (XRD) was performed on RIGAKU D/MAX 2550/PC diffractometer using Cu K_α radiation at 40 kV and 100 mA. Diffraction data was recorded using continuous scanning at 0.02°/s and a step size of 0.02°. Scanning electron microscope (SEM) images were obtained with a Zeiss Sigma field-emission SEM (Model 8100). Transmission electron microscopy (TEM, JEOL-2010 F) was used to observe the morphologies and dimensions of catalysts

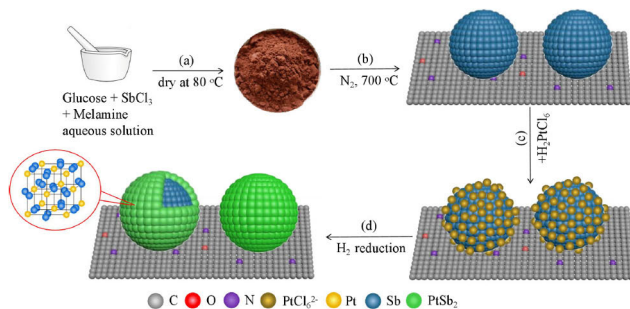


Fig. 1. Schematic illustration of the synthesis of catalysts.

Table 1

The textural structure and composition of catalysts.

Catalyst	Surface area (m ² /g)	Pore volume (cm ³ /g)	ICP loading ^a (wt.%)		XPS composition ^b (at.%)		
			Pt	Sb	N	O	C
Pt/C	115	0.065	4.41	0	0	20.87	78.82
Pt/NC	144	0.078	5.64	0	1.76	21.93	75.92
Sb@Pt/C	264	0.159	5.79	9.93	0	22.00	74.96
Sb@PtSb ₂ /NC	275	0.200	6.03	11.03	1.77	19.15	75.46

^a Detected via ICP analysis. ^b Detected via XPS.

at an accelerating voltage of 200 kV. X-ray photoelectron spectra (XPS) were recorded on a Perkin-Elmer PHI ESCA System. The X-ray source was a Mg standard anode 146 (1253.6 eV) operated at 12 kV and 300 W.

Oxygen adsorption and activation were measured over these catalysts via temperature programmed desorption of O₂ (O₂-TPD). The catalyst precursor was first pretreated at 700 °C in a purified H₂ flow of 30 mL/min for 1 h, and then the reactor was cooled to 50 °C in a H₂ atmosphere. Then, the synthesized catalyst was purged in a purified Ar flow of 30 mL/min at 50 °C for 1 h. After that, the catalyst was exposed to 10% O₂/Ar for 30 min, and then purged with Ar for 60 min at 50 °C in order to eliminate any physically adsorbed O₂. The desorption of adsorbed oxygen was conducted by ramping the catalyst temperature to 600 °C at a rate of 10 °C/min, and O₂ (*m/e* = 32) was detected in the effluent and recorded as a function of temperature using a quadrupole mass spectrometer (Omni Star TM, GSD301, Switzerland).

2.3. Glycerol oxidation

Glycerol oxidation was carried out in a 25-mL custom-designed stainless-steel autoclave with a glass inner layer, which contained 5 mL of a 0.2 g/mL glycerol solution and 0.100 g of catalyst. The reactor was sealed, filled with 0.6 MPa of O₂, placed in water bath preheated to the required temperature, and maintained at that temperature for a given time under vigorous stirring with a magnetic stirrer. After the reaction, the catalyst was removed by centrifugation and the aqueous solution was analyzed using a high-performance liquid chromatograph (HPLC, Agilent 1100 series) equipped with a refractive index detector (RID) and a Zorbax SAX column (4.6 mm × 250

mm, Agilent). The analysis procedures are described in detail in our previous work [42]. The selectivity of each product was calculated as: (mmol of product in reaction mixture) × (the number of carbon atoms in product) / ((initial mmol of glycerol – mmol of glycerol left) × 3) × 100%.

3. Results and discussion

3.1. Characterization

Fig. 2 shows the N₂ adsorption isotherms and pore size distributions of Pt/C, Pt/NC, Sb@Pt/C, and Sb@PtSb₂/NC. All catalysts were found to exhibit type I pattern isotherms, according to the International Union of Pure and Applied Chemistry (IUPAC) classification, which suggested that they were typical microporous materials. On the basis of adsorption data, the calculated BET surface areas of Pt/C, Pt/NC, Sb@Pt/C, and Sb@PtSb₂/NC were 115, 144, 264, and 275 m²/g, respectively. These results indicate that introducing N and/or Sb into the precursor (by adding melamine and/or SbCl₃) can increase the surface area and pore volume of the prepared catalyst. In addition, the effect of introducing Sb to the carbon support can be observed clearly in their typical SEM images. The outlines of Pt/C and Pt/NC look like closely packed solid laminates (see Fig. 3a–3d), while Sb@Pt/C and Sb@PtSb₂/NC exhibited porous structures (see Fig. 3e–3h).

Fig. 4 compares the XRD patterns of Pt/C, Pt/NC, Sb@Pt/C and Sb@PtSb₂/NC. It can be seen that the main diffraction peaks of Pt were detected in Pt/C and Pt/NC, while the calculated Pt crystallite sizes based on the full-width at half-maximum of the Pt(111) peak were 36.2 and 32.5 nm, respectively. These results indicate that introducing N into the

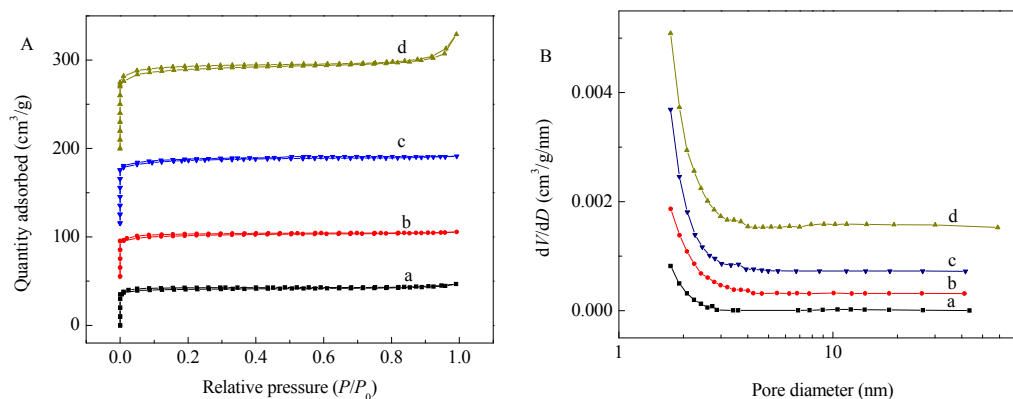


Fig. 2. (A) N₂ adsorption-desorption isotherms and (B) pore size distributions of (a) Pt/C, (b) Pt/NC, (c) Sb@Pt/C, and (d) Sb@PtSb₂/NC.

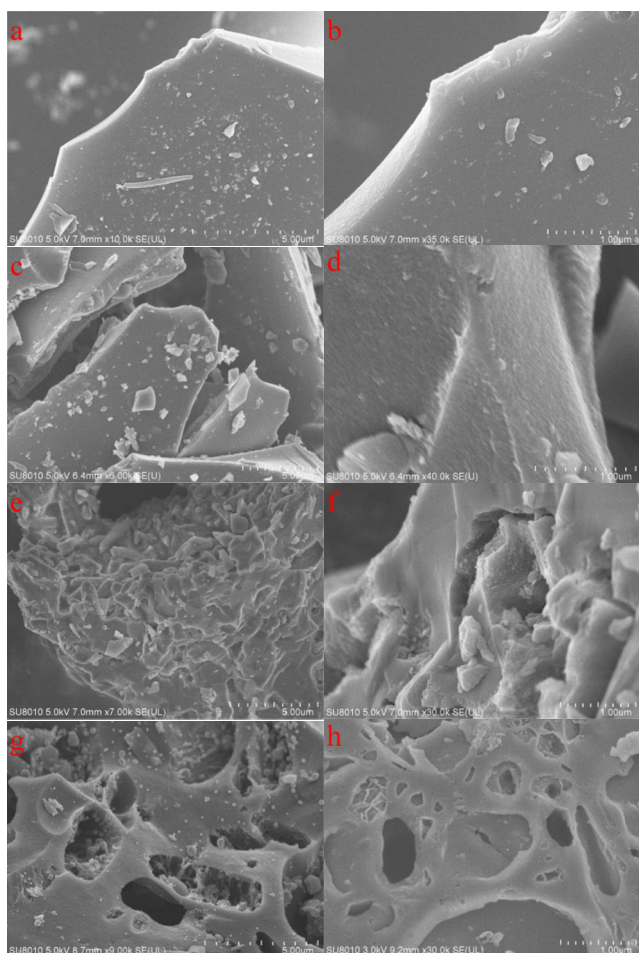


Fig. 3. SEM images of (a,b) Pt/C, (c,d) Pt/NC, (e,f) Sb@Pt/C, and (g,h) Sb@PtSb₂/NC.

catalyst can improve the dispersion of Pt, which might be attributed to the fact that N can increase the surface area of the carbon support and induce defects in the carbon support, strengthening the interactions between Pt and the carbon

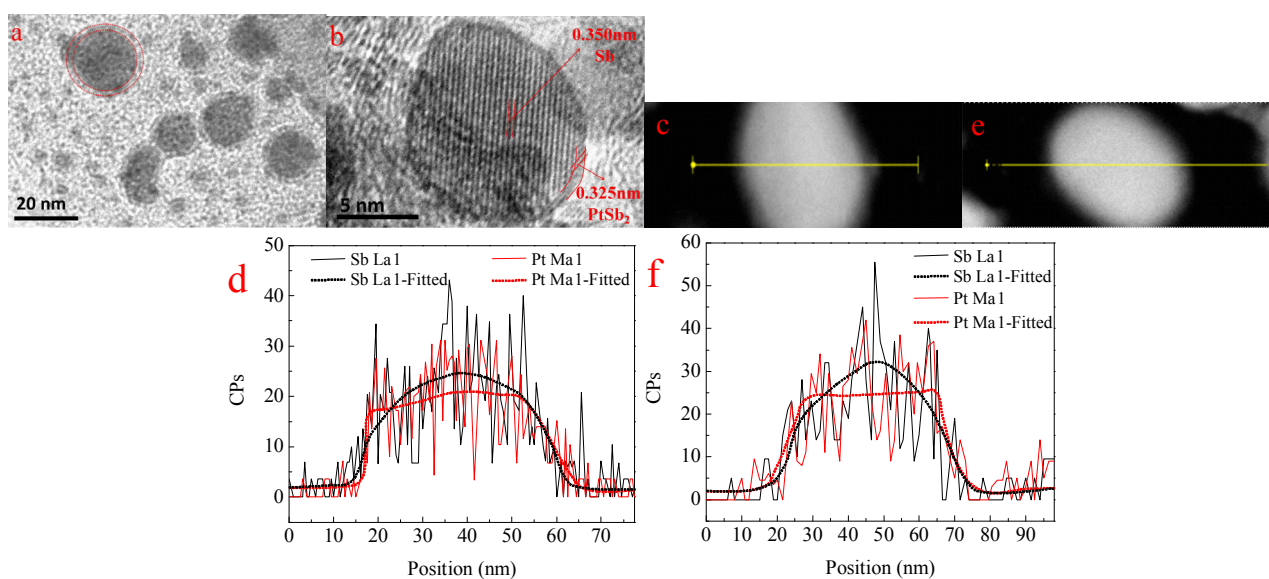


Fig. 5. TEM images and EDS spectra of Sb@PtSb₂/NC.

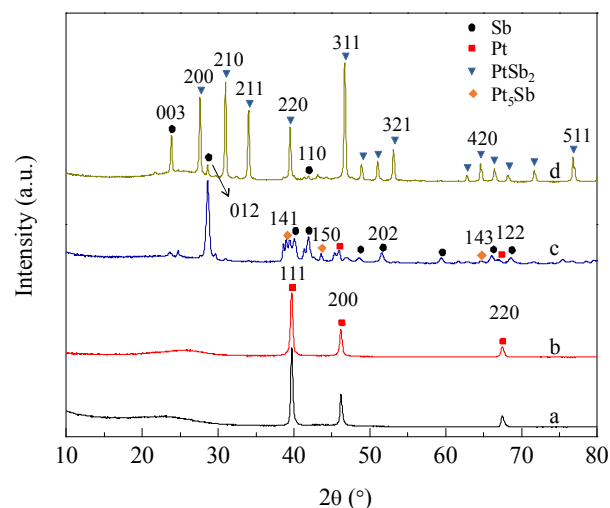


Fig. 4. XRD patterns of (a) Pt/C, (b) Pt/NC, (c) Sb@Pt/C, and (d) Sb@PtSb₂/NC.

support [42]. At the same time, it is interesting to note that a PtSb₂ alloy (JCPDS 14-0141) was detected in the Sb@PtSb₂/NC catalyst along with metallic Sb (JCPDS 35-0732), which means that Pt can enter into the lattice of Sb. Peaks around 23.8° and 28.6° confirmed the existence of a separate Sb phase. On the other hand, separate Sb and Pt phases and trace amounts of Pt₃Sb alloy were detected in the XRD pattern of Sb@Pt/C.

Typical HRTEM images indicated that a layer of PtSb₂ alloy formed on the surfaces of well-crystallized Sb particles in the Sb@PtSb₂/NC catalyst (see Fig. 5), as the observed d-spacing values of 0.325 nm and 0.350 nm correspond to the (200) plane of PtSb₂ alloy and the (101) plane of Sb (see Fig. 5b), respectively. Line-scan EDS results further confirmed that Pt was mainly located in the shell of the Sb@PtSb₂ hybrid (see Fig. 5c–5f).

Raman analysis further confirmed that introducing SbCl₃ into the mixture of glucose and melamine can induce defects in the final catalyst (see Fig. 6), as the calculated intensity ratio of

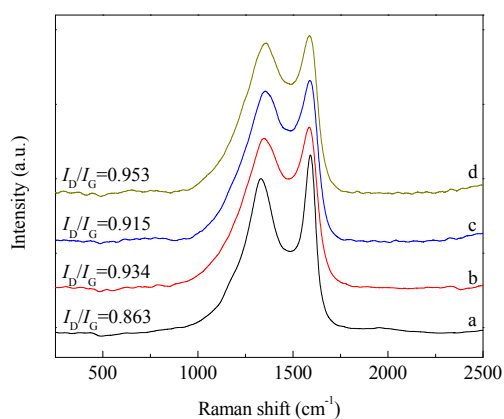


Fig. 6. Raman spectra of (a) Pt/C, (b) Pt/NC, (c) Sb@Pt/C, and (d) Sb@PtSb₂/NC.

the D band to G band (I_D/I_G) increased from 0.863 (in Pt/C) to 0.915 (in Sb@Pt/C), 0.934 (in Pt/NC), and 0.953 (in Sb@PtSb₂/NC). In addition, the introduction of N can also increase the amount of carbon defects, as the ratio of the D band to the G band (I_D/I_G) of Pt/NC increased compared to that of Pt/C. And these defects can bring additional active sites, which encourages the oxidation reaction [29,43].

Temperature-programmed desorption of O₂ (O₂-TPD, see Fig. 7) over Pt/NC and Sb@PtSb₂/NC catalysts indicated that mainly atomic oxygen was adsorbed on the surface of both catalysts [44,45], but the amount of desorbed O₂ over Sb@PtSb₂/NC was much higher than that over Pt/NC. The above XRD analysis indicated that the crystalline structure of the PtSb₂ alloy consists of a Pa-3 unit cell structure with a dimension of 0.644 nm (see Fig. 4), while the crystalline structure of elemental Pt consists of an Fm-3m unit cell structure with a dimension of 0.392 nm. The enhanced activation of oxygen over the Sb@PtSb₂ catalyst might be attributed to the formation of a PtSb₂ alloy shell and the enlarged distance between Pt atoms, which are more favorable for the dissociative adsorption of oxygen (see Fig. 7). In other words, the formation of a PtSb₂ alloy shell in the Sb@PtSb₂ hybrid increased the space between metal atoms, allowing the adsorption and surface diffusion of more oxygen atoms in the catalyst.

XPS analysis provided evidence of electron transfer from N

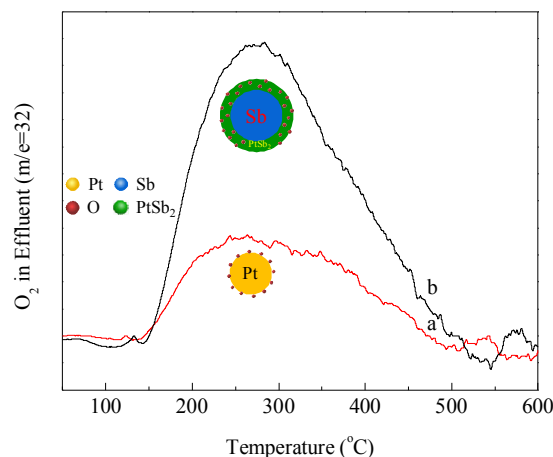


Fig. 7. O₂-TPD profiles of (a) Pt/NC and (b) Sb@PtSb₂/NC catalysts.

to Pt, as the detected binding energy of the Pt 4f peaks shifted from 71.4 and 74.7 eV (in Pt/C) to 71.0 and 74.3 eV (in Pt/NC), and from 71.3 and 74.6 eV (in Sb@Pt/C) to 70.8 and 74.1 eV (in Sb@PtSb₂/NC) (see Fig. 8A and 8B). At the same time, XPS also confirmed the formation of a PtSb₂ alloy in Sb@PtSb₂/NC, as the detected binding energy of Pt 4f in Sb@PtSb₂/NC falls well within the range of values reported for PtSb₂ in the literature [35]. Deconvolution of the N 1s spectra (see Fig. 8C) suggested the formation of pyridinic nitrogen (N1, 398.5 eV), pyrrolic nitrogen (N2, 400.1 eV), quaternary nitrogen (N3, 401.1 eV), and pyridine N-oxide nitrogen (N4, 403.3 eV) in Pt/NC and Sb@PtSb₂/NC [42]. It was reported that pyridinic N can reduce the energy barrier for the adsorption of reactants on adjacent carbon atoms and accelerate the rate-limiting first-electron transfer process, resulting in a significant enhancement of catalytic activity of the carbon surface [46,47]. Moreover, quaternary N in a graphene structure can bring about a non-uniform electron distribution and a significant enhancement of the catalytic activity of the carbon surface [48]. Introducing Sb and N dopants into the catalyst can enhance the interactions between Pt NPs and the carbon support, leading to an easier transfer of electrons from N atoms to Pt NPs, and these electron-enriched Pt particles are more active in the oxidation of glycerol.

The above characterizations confirmed that N-doped carbon-supported Sb@PtSb₂ hybrids with a core-shell structure

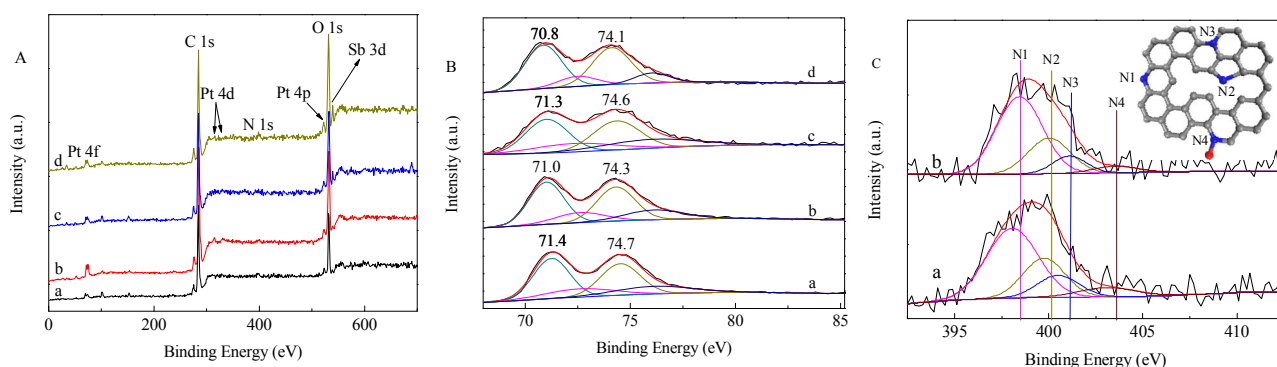


Fig. 8. (A) XPS spectra of (a) Pt/C, (b) Pt/NC, (c) Sb@Pt/C, and (d) Sb@PtSb₂/NC; (B) The BE of the Pt 4f peak in (a) Pt/C, (b) Pt/NC, (c) Sb@Pt/C, and (d) Sb@PtSb₂/NC; (C) The BE of the N 1s peak in (a) Pt/NC and (b) Sb@PtSb₂/NC.

could be fabricated in a facile manner via the direct pyrolysis of a mixture of glucose, melamine, and SbCl_3 , followed by impregnation with Pt.

3.2. Catalytic activity for selective oxidation of glycerol

Catalytic reaction results confirmed that this $\text{Sb@PtSb}_2/\text{NC}$ catalyst was highly active for the selective oxidation of glycerol in base-free aqueous solutions. As is summarized in Table 2, Sb/NC was inactive for the oxidation of glycerol, which indicates that Pt and/or PtSb_2 provide the active sites for this reaction. The detected conversion of glycerol over the monometallic Pt/C catalyst was low (13.5%), and mainly GLYA (75.2%), DHA (12.8%), and HPYA (5.6%) were detected. The conversion of glycerol over Pt/NC improved significantly to 21.5% with 77.3% selectivity for GLYA. The higher activity of Pt/NC may be attributed to its higher surface area, increased amount of carbon defects, and higher dispersion of Pt, while electron donation from N to Pt can also accelerate the activation of molecular oxygen and improve the reaction rate. When Sb was added to the catalyst ($\text{Sb@Pt}/\text{C}$), the conversion of glycerol further increased to 26.0% with a 73.3% selectivity for GLYA. It is interesting to note that the detected conversion of glycerol jumped to 65.3% over $\text{Sb@PtSb}_2/\text{NC}$ under the same reaction conditions, and the selectivity for DHA increased to 39.2%. The calculated TOF value on the basis of total Pt metal in $\text{Sb@PtSb}_2/\text{NC}$ at a conversion of 10% reached 130.1 h^{-1} , which is higher than those of Pt/C (34.3 h^{-1}), Pt/NC (67.0 h^{-1}), and $\text{Sb@Pt}/\text{NC}$ (76.3 h^{-1}) [49,50]. The enhanced activity of $\text{Sb@PtSb}_2/\text{NC}$ could be attributed to its higher surface area (see Fig. 2 and Table 1) and increased amount of surface defects, which promoted the adsorption and activation of glycerol and oxygen. At the same time, the formation of a PtSb_2 alloy in $\text{Sb@PtSb}_2/\text{NC}$ was also favorable for the adsorption and transfer of oxygen (see the O_2 -TPD in Fig. 7). It was also found that the Sb@PtSb_2 hybrid was more selective for the formation of DHA, which might be attributed to the fact that the PtSb_2 alloy can suppress the further oxidation of DHA (see Fig. 9) [40].

Fig. 9 shows the time course of glycerol oxidation over $\text{Sb@PtSb}_2/\text{NC}$ at 60°C in 0.2 g/mL glycerol aqueous solution. It can be seen that the conversion of glycerol increased quickly to

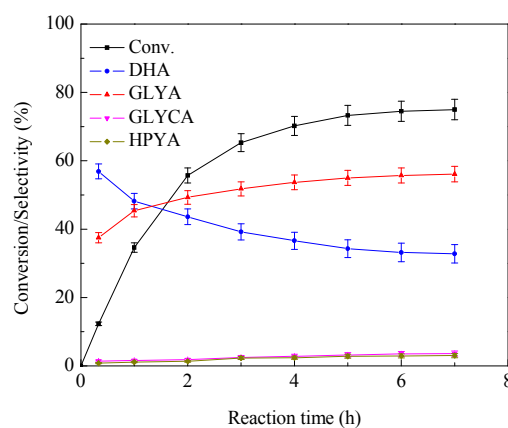


Fig. 9. Time course of glycerol oxidation over $\text{Sb@PtSb}_2/\text{NC}$.

70.2% within the first four hours, and then increased steadily in the following time. The reaction rate slowed down with increasing conversion, which might be caused by the strong adsorption of the formed products. This phenomenon was discussed by Davis et al. in 2014 [23], and several works from Zhou et al. also confirmed that strongly adsorbed intermediates can decrease the reaction rate over Pt/AC(PO) catalysts [51,52]. When these adsorbed intermediates were washed off, the $\text{Sb@PtSb}_2/\text{NC}$ catalyst could be recovered. At the same time, it was found that the selectivity to DHA reached 56.9% at the beginning of the reaction, and it decreased continuously with time on stream. These results indicate that DHA is an important intermediate of the reaction. The selectivity to GLYA increased from 37.5% (at the beginning of the reaction) to 70.2% (at 4 h), and then changed only slightly. On the other hand, the selectivity of HPYA and products derived from C–C bond cleavage (such as GLYCA) increased continuously. In this case, we think that the primary product DHA and/or GLYA would further oxidize to HPYA and GLYCA during the reaction. The proposed reaction network is illustrated in Fig. 10.

That is, GLY was first oxidized to DHA or GLYHD, then GLYHD was further oxidized to GLYA, and then GLYA could be oxidized to GLYCA, OXA, or even to CO_2 . At the same time, DHA was further oxidized to HPYA, and then HPYA could be oxidized to GOX, OXA, or even to CO_2 (see Fig. 10).

Fig. 11 shows the performance of the recycled $\text{Sb@PtSb}_2/\text{NC}$ catalyst for the selective oxidation of glycerol under base-free conditions. The conversion of glycerol decreased from 65.3% to 43.1% after the catalyst was used five times, while the selectivity of GLYA and DHA remained almost

Table 2

The performance for selective oxidation of glycerol^a.

Catalyst	Conv. (mol%)	TOF ^b (h^{-1})	Product selectivity ^c (mol%)				
			DHA	GLYA	GLYCA	HPYA	Others
Sb/NC	0	–	0	0	0	0	0
Pt/C	13.5	34.3	12.8	75.2	0	5.6	6.4
Pt/NC	21.5	67.0	13.2	77.3	0	4.3	5.2
Sb@Pt/C	26.0	76.3	14.5	73.3	0	3.8	8.4
Sb@PtSb ₂ /NC	65.3	130.1	39.2	51.8	2.5	2.3	4.2

^a Reaction conditions: catalyst loading of 0.100 g, 5 mL of 0.2 g/mL aqueous glycerol solution, 60°C , 0.6 MPa O_2 , 3 h.

^b Calculated on the basis of total Pt at a conversion of 10%.

^c Calculated as: (mmol of product in reaction mixture) \times (the number of carbon atoms in product) / ((initial mmol of glycerol – mmol of glycerol left) \times 3) \times 100%. GLYA: glyceric acid; DHA: 1,3-dihydroxyacetone; GLYCA: glycolic acid; HPYA: hydroxy-pyruvic acid.

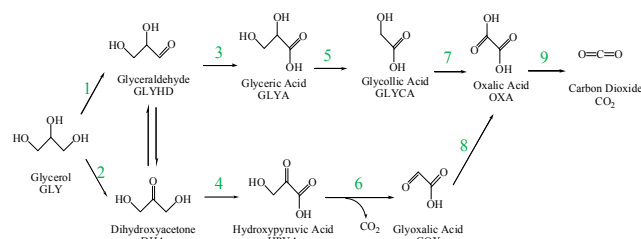


Fig. 10. The glycerol oxidation network.

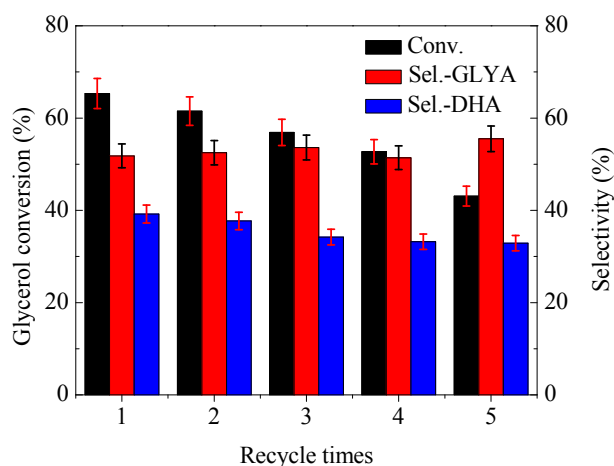


Fig. 11. The conversion of glycerol over recycled Sb@PtSb₂/NC. (■) glycerol conversion; (■) selectivity of GLYA; (■) selectivity of DHA. Reaction conditions: catalyst Sb@PtSb₂/NC, 0.2 g/mL aqueous glycerol solution (initial glycerol/Pt = 351), 0.6 MPa O₂, 3 h.

the same. These results show that Sb@PtSb₂/NC still maintained high activity for the oxidation of glycerol after five cycles. The deactivation might be attributed to the mass loss of the catalyst during the reaction and recycling process because of the vigorous stirring involved.

4. Conclusions

Sb@PtSb₂ hybrids with a core-shell structure could be fabricated on the surface of N-doped carbon (NC) via a facile synthesis route. It was confirmed that SbCl₃ can increase the surface area of a binary glucose + melamine pyrolyzed support, and a PtSb₂ alloy shell could be formed on the surface of Sb particles during the hydrogen reduction. The synthesized Sb@PtSb₂ hybrid was more active for the absorption and activation of O₂, and also exhibited prominent activity for the selective oxidation of glycerol with molecular oxygen. The best spe-

cific activity based on the total amount of Pt reached 130.1 h⁻¹.

References

- [1] A. Talebian-Kiakalaieh, N. A. S. Amin, K. Rajaei, S. Tarighi, *Appl. Energy*, **2018**, 230, 1347–1379.
- [2] L. H. Yang, X. W. Li, P. Chen, Z. Y. Hou, *Chin. J. Catal.*, **2019**, 40, 1020–1034.
- [3] K. Kong, D. F. Li, W. B. Ma, Q. Q. Zhou, G. P. Tang, Z. S. Hou, *Chin. J. Catal.*, **2019**, 40, 534–542.
- [4] C. Zhang, T. Wang, Y. J. Ding, *Chin. J. Catal.*, **2017**, 38, 928–938.
- [5] M. Y. Zhang, Y. Y. Sun, J. J. Shi, W. S. Ning, Z. Y. Hou, *Chin. J. Catal.*, **2017**, 38, 537–544.
- [6] T. Jedsukontorn, V. Meeyoo, N. Saito, M. Hunsom, *Chin. J. Catal.*, **2016**, 37, 1975–1981.
- [7] M. L. Faroppa, J. J. Musci, M. E. Chiosso, C. G. Caggiano, H. P. Bideberripe, J. L. García Fierro, G. J. Siri, M. L. Casella, *Chin. J. Catal.*, **2016**, 37, 1982–1990.
- [8] H. Kimura, K. Tsuto, T. Wakisaka, Y. Kazumi, Y. Inaya, *Appl. Catal. A: Gen.*, **1993**, 96, 217–228.
- [9] P. Gallezot, *Catal. Today*, **1997**, 37, 405–418.
- [10] S. Carretin, P. McMorn, P. Johnston, K. Griffin, C. J. Kiely, G. J. Hutchings, *Phys. Chem. Chem. Phys.*, **2013**, 5, 1329–1336.
- [11] B. N. Zope, D. D. Hibbitts, M. Neurock, R. J. Davis, *Science*, **2010**, 330, 74–78.
- [12] M. S. Ide, R. J. Davis, *Acc. Chem. Res.*, **2014**, 47, 825–833.
- [13] A. Villa, N. Dimitratos, C. E. Chan-Thaw, C. Hammond, L. Prati, G. J. Hutchings, *Acc. Chem. Res.*, **2015**, 48, 1403–1412.
- [14] Y. Li, F. Zaera, *J. Catal.*, **2015**, 326, 116–126.
- [15] J. Dou, B. W. Zhang, H. Liu, J. D. Hong, S. M. Yin, Y. Z. Huang, R. Xu, *Appl. Catal. B: Environ.*, **2016**, 180, 78–85.
- [16] Z. F. Yuan, Z. K. Gao, B. Q. Xu, *Chin. J. Catal.*, **2015**, 36, 1543–1551.
- [17] C. L. Xu, Y. Q. Du, C. Li, J. Yang, G. Yang, *Appl. Catal. B: Environ.*, **2015**, 164, 334–343.
- [18] A. Villa, S. Campisi, K. M. H. Mohammed, N. Dimitratos, F. Vindigni, M. Manzoli, W. Jones, M. Bowker, G. J. Hutchings, L. Prati, *Catal. Sci. Technol.*, **2015**, 5, 1126–1132.
- [19] Y. Li, F. Zaera, *Catal. Sci. Technol.*, **2015**, 5, 3773–3781.
- [20] E. Skrzyńska, S. Zaid, A. Addad, J.-S. Girardon, M. Capron, F. Dumeignil, *Catal. Sci. Technol.*, **2016**, 6, 3182–3196.

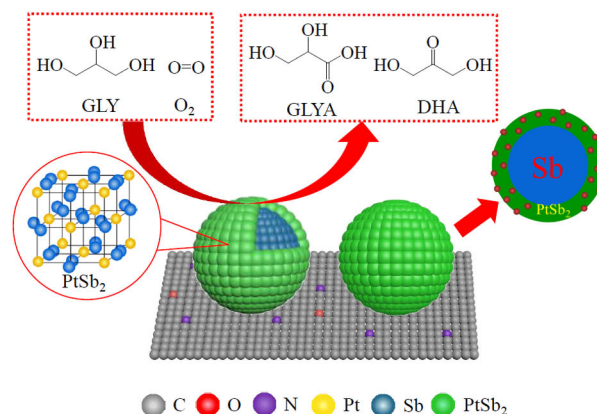
Graphical Abstract

Chin. J. Catal., 2020, 41: 494–502 doi: S1872-2067(19)63476-5

Selective oxidation of glycerol with oxygen in base-free solution over N-doped-carbon-supported Sb@PtSb₂ hybrid

Lihua Yang, Tianqu He, Chujun Lai, Ping Chen, Zhaoyin Hou*
Zhejiang University

An Sb@PtSb₂ hybrid catalyst with a core-shell structure was fabricated on the surface of N-doped carbon (NC) via a facile synthesis route, which exhibited prominent activity for the selective oxidation of glycerol with molecular oxygen.



- [21] G. Dodekatos, H. Tüysüz, *Catal. Sci. Technol.*, **2016**, 6, 7307–7315.
- [22] G. Dodekatos, J. Ternieden, S. Schünemann, C. Weidenthaler, H. Tüysüz, *Catal. Sci. Technol.*, **2018**, 8, 4891–4899.
- [23] M. S. Ide, D. D. Falcone, R. J. Davis, *J. Catal.*, **2014**, 311, 295–305.
- [24] S. S. Chen, P. Y. Qi, J. Chen, Y. Z. Yuan, *RSC Adv.*, **2015**, 5, 31566–31574.
- [25] Y. Y. Sun, X. W. Li, J. G. Wang, W. S. Ning, J. Fu, X. Y. Lu, Z. Y. Hou, *Appl. Catal. B: Environ.*, **2017**, 218, 538–544.
- [26] A. Villa, G. M. Veith, L. Prati, *Angew. Chem. Int. Ed.*, **2010**, 49, 4499–4502.
- [27] G. L. Brett, Q. He, C. Hammond, P. J. Miedzak, N. Dimitratos, M. Sankar, A. A. Herzing, M. Conte, J. A. Lopez-Sanchez, C. J. Kiely, D. W. Knight, S. H. Taylor, G. J. Hutchings, *Angew. Chem. Int. Ed.*, **2011**, 50, 10136–10139.
- [28] C. M. Olmos, L. E. Chinchilla, E. G. Rodrigues, J. J. Delgado, A. B. Hungria, G. Blanco, M. F. R. Pereira, J. J. M. Órfã, J. J. Calvino, X. W. Chen, *Appl. Catal. B: Environ.*, **2016**, 197, 222–235.
- [29] W. B. Hu, B. Lowry, A. Varma, *Appl. Catal. B: Environ.*, **2011**, 106, 123–132.
- [30] J. B. Goodenough, R. Manoharan, A. K. Shukla, K. V. Ramesh, *Chem. Mater.*, **1989**, 1, 391–398.
- [31] J. H. Kim, S. M. Choi, S. H. Nam, M. H. Seo, S. H. Choi, W. B. Kim, *Appl. Catal. B: Environ.*, **2008**, 82, 89–102.
- [32] M. J. González, C. T. Hable, M. S. Wrighton, *J. Phys. Chem. B*, **1998**, 102, 9881–9890.
- [33] K. W. Park, J. H. Choi, B. K. Kwon, S. A. Lee, Y. E. Sung, H. Y. Ha, S. A. Hong, H. Kim, A. Wieckowski, *J. Phys. Chem. B*, **2002**, 106, 1869–1877.
- [34] M. Y. Zhang, J. J. Shi, W. S. Ning, Z. Y. Hou, *Catal. Today*, **2017**, 298, 234–240.
- [35] R. F. Nie, D. Liang, L. Shen, J. Gao, P. Chen, Z. Y. Hou, *Appl. Catal. B: Environ.*, **2012**, 127, 212–220.
- [36] X. M. Ning, Y. H. Li, H. Yu, F. Peng, H. J. Wang, Y. H. Yang, *J. Catal.*, **2016**, 335, 95–104.
- [37] O. S. G. P. Soares, R. P. Rocha, A. G. Gonçalves, J. L. Figueiredo, J. J. M. Órfã, M. F. R. Pereira, *Appl. Catal. B: Environ.*, **2016**, 192, 296–303.
- [38] X. M. Ning, Y. H. Li, B. Q. Dong, H. J. Wang, H. Yu, F. Peng, Y. H. Yang, *J. Catal.*, **2017**, 348, 100–109.
- [39] D. H. Guo, R. Shibuya, C. Akiba, S. Saji, T. Kondo, J. Nakamura, *Science*, **2016**, 351, 361–365.
- [40] X. Z. Duan, Y. F. Zhang, M. J. Pan, H. Dong, B. X. Chen, Y. Y. Ma, G. Qian, X. G. Zhou, J. Yang, D. Chen, *AIChE J.*, **2018**, 64, 3979–3987.
- [41] D. Liang, J. Gao, H. Sun, P. Chen, Z. Y. Hou, X. M. Zheng, *Appl. Catal. B: Environ.*, **2011**, 106, 423–432.
- [42] L. H. Yang, X. W. Li, Y. Y. Sun, L. H. Yue, J. Fu, X. Y. Lu, Z. Y. Hou, *Catal. Commun.*, **2017**, 101, 107–110.
- [43] M. Li, Y. P. Xiong, X. T. Liu, C. Han, Y. F. Zhang, X. J. Bo, L. P. Guo, *J. Mater. Chem. A*, **2015**, 3, 9658–9667.
- [44] A. Katsaounis, Z. Nikopoulou, X. E. Verykios, C. G. Vayenas, *J. Catal.*, **2004**, 222, 192–206.
- [45] X. Fu, Y. Liu, W. Yao, Z. Wu, *Catal. Commun.*, **2016**, 83, 22–26.
- [46] Q. G. He, Q. Li, S. Khene, X. M. Ren, F. E. López-Suárez, D. Lozano-Castelló, A. Bueno-López, G. Wu, *J. Phys. Chem. C*, **2013**, 117, 8697–8707.
- [47] G. Wu, K. L. More, P. Xu, H. L. Wang, M. Ferrandon, A. J. Kropf, D. J. Myers, S. G. Ma, C. M. Johnston, P. Zelenay, *Chem. Commun.*, **2013**, 49, 3291–3293.
- [48] M. Xiao, J. Zhu, L. Feng, C. Liu, W. Xing, *Adv. Mater.*, **2015**, 27, 2521–2527.
- [49] S. Kozuch, J. M. L. Martin, *ACS Catal.*, **2012**, 2, 2787–2794.
- [50] F. Schüth, M. D. Ward, J. M. Buriak, *Chem. Mater.*, **2018**, 30, 3599–3600.
- [51] J. Q. Lei, H. Dong, X. Z. Duan, W. Y. Chen, G. Qian, D. Chen, X. G. Zhou, *Ind. Eng. Chem. Res.*, **2016**, 55, 420–427.
- [52] J. Q. Lei, X. Z. Duan, G. Qian, X. G. Zhou, *CIESC*, **2017**, 68, 679–686.

氮掺杂碳负载Sb@PtSb₂催化剂的制备及其在甘油选择性氧化反应中的应用

杨丽华^a, 何天衢^a, 赖楚钧^a, 陈平^a, 侯昭胤^{a,b,*}

^a浙江大学化学系生物物质化工教育部重点实验室, 浙江杭州310028

^b浙江大学化学系化学前瞻技术研究中心, 浙江杭州310028

摘要: 甘油是生物柴油生产过程中生成的副产物, 随着生物柴油产量的快速增长, 甘油的量也迅速增加。据估计, 到2020年甘油的产量将比需求量高出6倍。因此, 将过剩的甘油转化为其它更有价值的化学品具有重要意义。

在已经发表的文献中, 各种碳材料负载的Pt催化剂被广泛应用于液相中甘油的选择性氧化。但是, 由于Pt纳米颗粒与碳载体之间相互作用较弱, 因此Pt纳米颗粒易团聚和流失, 而且Pt的过度氧化和有机羧酸的强吸附也导致Pt催化剂失活。最近的研究表明, 采用含氮的碳载体可以增强Pt与载体间的相互作用, 这种载体还有可能将电子转移给Pt, 从而有效提高Pt的分散度、活性和稳定性。与此同时, 引入其它金属如Co, Cu, Bi, Sb等与Pt形成合金也能有效改善催化剂的活性和稳定性。我们在前期工作中曾经发现多壁碳纳米管(MWCNTs)负载的PtSb合金在甘油氧化反应中具有很高的活性和二羟基丙酮选择性, 可以抑制C–C裂解, 并提高了催化剂的稳定性。但是在MWCNTs上组装PtSb颗粒的过程繁琐且危险, 需要对载体进行氧化(浓硝酸)、嫁接硫醇、浸渍金属、高温还原等, 同时MWCNTs的价格也较高。

本文采用简单的热解方法将氮和锑同时引入到碳基载体中, 并用此载体制备了具有核壳结构的Sb@PtSb₂/NC催化剂。首先将葡萄糖、三聚氰胺和SbCl₃混合后在氮气中于700 °C热解得到含Sb和N的多孔碳载体, 再通过浸渍还原法将Pt还原并负载到该载体上即得到具有核壳结构的Sb@PtSb₂/NC催化剂。该催化剂对催化甘油氧化具有较高的活性, 同时具有较好的稳定性。氮气吸附表征表明, 引入N和Sb都能提高载体的比表面积和孔体积, 其中Sb的引入使得催化剂表面形成了多孔结构(SEM表征)。XRD、TEM和EDS表征证明了具有核壳结构的Sb@PtSb₂颗粒在载体表面上的生成。Raman光谱表明N和Sb的引入增加了碳缺陷, 有可能带来新的活性位点。O₂-TPD表征表明Sb@PtSb₂/NC对氧的吸附量远高于Pt/NC, 这可能归因于PtSb₂合金中Pt-Sb金属间的原子间距增大, 有利于氧的吸附和表面扩散, 从而显著提高了催化剂活性。XPS表征表明了从

N到Pt的电子转移,而这种富含电子的Pt具有更高的活性.将制备的催化剂用于考评催化甘油氧化的活性,发现相比于Pt/NC, Sb@PtSb₂/NC催化剂催化甘油氧化具有显著增加的活性,二羟基丙酮选择性也明显提高,在60 °C, 0.6 MPa O₂气氛下, 100 mg催化剂与5 mL 0.2 g/mL甘油水溶液反应3 h得到了65.3%的甘油转化率,以及39.2%的二羟基丙酮选择性和51.8%的甘油酸选择性.这可能归因于载体比表面积的增加、更多的碳缺陷,以及PtSb₂合金的形成.使用五次后的催化剂仍保持较高的催化活性,证实了该催化剂具有较好的稳定性.

关键词: 甘油; 氧化; 无碱溶液; Sb@PtSb₂; 合金

收稿日期: 2019-07-04. 接受日期: 2019-08-06. 出版日期: 2020-03-05.

*通讯联系人. 电子信箱: zyhou@zju.edu.cn

基金来源: 国家自然科学基金(21773206, 21473155); 浙江省自然科学基金(L12B03001).

本文的电子版全文由Elsevier出版社在ScienceDirect上出版(<http://www.sciencedirect.com/science/journal/18722067>).